Combined computed nanotomography and nanoscopic x-ray fluorescence imaging of cobalt nanoparticles in caenorhabditis elegans

Article

Combined nano-CT and nano-XRF imaging of cobalt nanoparticles in Caenorhabiditis elegans

Simone Cagno, Dag Anders Brede, Gert Nuyts, Frederik Vanmeert, Alexandra Pacureanu, Remi Tucoulou, Peter Cloetens, Gerald Falkenberg, Koen Janssens, Brit Salbu, and Ole Christian Lind

Anal. Chem., **Just Accepted Manuscript** • DOI: 10.1021/acs.analchem.7b02554 • Publication Date (Web): 10 Oct 2017

Combined nano-CT and nano-XRF imaging of cobalt nanoparticles in Caenorhabiditis elegans

Simone Cagno[a*$], Dag Anders Brede[a$], Gert Nuyts[b], Frederik Vanmeert[b], Alexandra Pacureanu[c], Remi Tucoulou[c], Peter Cloetens[c], Gerald Falkenberg[d], Koen Janssens[b], Brit Salbu[a], Ole Christian Lind[a],

[a.] CERAD CoE, Faculty of Environmental Sciences and Natural Resource Management, Norwegian University of Life Sciences, P.O. Box 5003, 1432 Ås, Norway

[b.] University of Antwerp, Department of Chemistry, Groenenborgerlaan 171, 2020 Antwerpen, Belgium

[c.] ESRF, 71 Avenue des Martyrs, 38000 Grenoble, France

[d.]DESY, Notkestrasse 85, 22607 Hamburg, Germany

ABSTRACT: Synchrotron radiation phase contrast nano-CT and (2D and 3D) nano-XRF were used to investigate the internal distribution of engineered Co nanoparticles in exposed individuals of the nematode *Caenorhabiditis elegans*. Whole nematodes and selected tissues and organs were 3D rendered: anatomical 3D renderings with 50 nm voxel size enabled the visualization of 50-200 nm sized, spherical nanoparticle aggregates within intact *C. elegans*. A 20 x 37 nm^2 high-brilliance beam was employed to obtain XRF elemental distribution maps of entire nematodes or anatomical details such as embryos, which could be compared with the CT data. These maps showed Co-NPs to be predominantly present within the intestine and the epithelium, and were not co-localized with the Zn granules found in the lysosomal containing vesicles or Fe agglomerates in the intestine. Iterated XRF-scanning of a specimen at 0 and 90 degree angles suggested that NP-aggregates were translocated into tissues outside of the intestinal lumen. Virtual slicing by means of 2D XRF tomography, combined with holotomography indicated presumable presence of individual NP-aggregates inside the uterus and within embryos.

Introduction

Adequate characterization of exposure is highly needed within nanotoxicology. In particular, the combination of morphological information at the nanometer level with elemental distribution at the same resolution, would greatly improve current knowledge of the fate of nanoparticles (NPs) in exposed organisms[1]. Such highly detailed information can be provided by X-ray nanoimaging, while at the same time preserving the physical integrity of the samples.

X-ray absorption and phase contrast tomography are non-invasive techniques used for morphological investigations, which allow quite flexible sample environments. For instance, biota can be readily imaged, entirely or locally[1-4]. A (sub)micrometer spatial resolution is typically achievable with laboratory based equipment, but this is not sufficient for characterization of NPs in toxicology, as it does not allow to image the distribution of single NPs or small aggregates of NPs within organisms. Currently, phase contrast and X-ray attenuation information collected in the 10-100 nm resolution range is state-of-the-art for nanoparticle exposure studies, and is only available at a few synchrotron beamlines[5,6,7].

Synchrotron-based X-ray fluorescence is another non-invasive technique, which enables imaging the distribution of many major, minor and trace-level elements. These can be either biologically relevant, or deliberately introduced into tissues and cells, for example as nanoparticles. Nowadays, submicron resolution is achieved at several imaging beamlines worldwide, with resolution in the range of tens of nm[8,9]. The possibility of performing 2D XRF tomography, i.e. reconstructing one or multiple virtual cross-sections of the elemental distribution, is of particular interest for exposure studies. Whereas regular 2D XRF provides the projected elemental distribution across the sample thickness, thus not allowing to distinguish the in-depth distribution, XRF tomography provides elemental distributions of a virtual cross-section which give access to this valuable depth information. This makes it possible to identify for example surface contaminants or the positions of elements inside the organism.

The application of both the above-mentioned techniques with similar spatial resolution (i.e. below the 100 nm threshold) provides incommensurable benefits for nanoparticle studies, as it allows relating the detected foreign elements to their position in the organ/tissue of the exposed biota. The few studies reported in the literature present results based solely on 2D XRF[9,10]. Beamline ID16A at ESRF was constructed to facilitate such studies, providing both techniques in the same experimental station, with 20 x 37 nm^2 as the smallest achievable beam size[7,11].

Metal NPs are used in a wide range of industrial processes, clothing and household utensils, and they represent the majority of NP emissions to the environment. There is considerable uncertainty related to the potential hazards of NPs in the environment, particularly related to toxic effects in exposed organisms.

The toxicity of metal NPs is highly dependent on their physical and chemical properties, which determine their mobility in the environment, chemical reactivity, bioavailability, persistence inside organisms and interactions with biomolecules[10]. Metal NPs that are retained in organisms may cause toxic effects to tissues and organs, which ultimately harm the organism as a whole.

While evidence on toxic effects is abundant, and numerous adverse biological effects have been reported in much detail[12,13], information on the internal distribution of nanoparticles taken up by exposed organisms is scarce. Particularly, data on the mobility and interaction of NPs with critical organs and tissues within complete intact organisms are lacking.

Cobalt NPs are widely used in industrial and medical applications such as fabrication of catalysts, photovoltaics, magnetic recordings, contrast enhancement in magnetic resonance imaging (MRI) and drug delivery[14,15]. However, only a few studies have investigated their potential effects on exposed organisms. Previous investigations of physical, chemical and toxicological properties of commercially available Co NPs have shown that such particles were readily ingested by important soil species and that their uptake induced adverse effects[12,13]. Therefore, the study of the internal distribution and effects of the exposure of living organisms to Co (NPs) is highly relevant.

C. elegans is a widely used model organism to study uptake, fate and toxicity of a wide variety of NP[16]. In the environment, this nematode moves through the soil and feeds off bacteria and is as such part of the soil food web. *C. elegans* is domesticated and is an important model for soil toxicology. Due to their short life cycle, ease to grow in bulk population, their small size (~0.05 mm x 1 mm) and optical transparency, *C. elegans* (Figure 1) are an ideal target for the imaging of whole organisms, as well as of individual organs[17]. These features have also enabled the investigation of biometal distribution at μm resolution in the entire *C. elegans* by synchrotron radiation[18,19,20].

The classical methods for assessing NP in *C. elegans* include fluorescence microscopy on labeled particles[21]. Unlabeled particles have been visualized using hyperspectral imaging and invasive methods like transmission electron (TEM) microscopy[22]. *C. elegans* has also facilitated groundbreaking science on uptake and fate of NPs using the combination of classical fluorescence microscopy and μXRF[23]. This has shown that NPs behave differently within *C. elegans* depending on their size, surface charge and coating[24].

In order to investigate the accumulation and distribution of Co NPs within exposed soil invertebrates, we employed the *C. elegans* model. In this study we present the results of a first of a kind experiment, where synchrotron radiation 2D (tomo) XRF and CT were used to perform non-invasive chemical and morphological nanoimaging of entire nematodes exposed to Co NPs, in order to track individual NP-aggregates within an intact exposed organism.

Materials and Methods

Cobalt NanoParticles (Co NPs)

Co NPs (QSI-nano cobalt, 3.9 ± 0.8 nm) were obtained from a commercial provider (Quantum Sphere Santa Ana, CA, USA). Equilibrated suspensions (2 mg/L) of nanoparticles in SSPW (standard soil pore water)[25] were prepared immediately prior to exposure. The preparation of the nematodes for the exposure was conducted following a standardized toxicity test protocol, as explained in the SI[26]. Thus, only a brief description of the sample preparation is given here.

Preservation of nematodes for X-ray imaging analysis

Exposed adult nematodes were gently transferred to a 15 mL Nunc tube, centrifuged (280 x g, 1 min) at room temperature, supernatant aspirated and washed once in 5 mL of SSPW. Nematodes from selected samples were depurated by feeding on *E. coli* OP50 NGM agar plates for 2 hours, and subsequently washed in 5 mL of SSPW.

Washed nematodes were incubated in 0.05 M Pipes buffer (pH 7.0) for 10 min, centrifuged (280 x g, 1 min) and the supernatant was removed. Nematodes were subsequently incubated overnight in 2 mL of freshly prepared fix solution (2% paraformaldehyde + 1.25% glutaraldehyde in 0.05 M PIPES buffer, pH 7.0). The samples were washed 3 times in 0.05 M PIPES buffer, pH 7.0, with 10 min incubation between each step. Nematodes were then mounted inside 0.1 mm diameter Quartz (Hampton Research, Ca, USA) or PMMA (Paradigm Optics, Vancouver, Ca.) capillaries prepared by coating with 1mg/mL polylysine (Sigma). Mounted nematodes were dehydrated by stepwise 15 min incubation in 30-50-70-96 and 4 x 100% EtOH in sealed containers. Samples were immediately immersed in Hexamethyldisilasane (HDMS) (Sigma), which was allowed to evaporate overnight (Mounted sample shown in Figure S2).

Synchrotron based nanoscale X-ray phase-contrast tomography and X-ray fluorescence imaging

Phase contrast computed nano-tomography combined with nanoscopic regular scanning and tomographic X-ray Fluorescence (XRF) measurements were carried out at beamline ID16A of the ESRF (Grenoble, France). The beamline produces a highly brilliant X-ray nano-focused beam at specific energies (17 keV and 33.6 keV), suited for analytical imaging of samples relevant in biology, biomedicine, materials science and nano-technology[11]. The available techniques are holography, ptychography and X-ray fluorescence, both in 2D and in 3D. Further information about the beamline layout is provided in the Supplementary Information (Figure S1).

The selected beam energy was 17 keV, which enables the detection of a wide range of elements relevant in biology. For phase contrast imaging magnified holotomography was used[27], which enables to retrieve the local electron density in 3D. The sample is placed downstream of the beam focus at the position corresponding to the chosen pixel size, which is given by geometrical magnification. The intensity of the propagated beam is recorded with a CCD FReLoN detector (2048x2048 pixels) after conversion into visible light with a scintillator.

The samples were imaged with two voxel sizes, 130 nm and 50 nm, yielding fields of view of 260 μm^2 and 100 μm^2, respectively. A tomographic scan was recorded at four different distances from the focal spot. The combination of the four holograms for each angle enables a more precise phase shift reconstruction. For each scan 1000 projections (180 degrees) with an exposure time of 0.25 s were recorded. Regarding the image reconstruction, each set of four holograms corresponding to one rotation angle is brought to the same magnification and aligned, before introducing it into a phase retrieval algorithm. These steps of data processing are implemented in Octave. The obtained phase maps are then used for tomographic reconstruction via filtered back-projection (PyHST).

The original output of a (nano-)CT experiment is a stack of virtual slices or tomograms, but in order to fully appreciate the information contained it is often visualized as 3D renderings (Figure 1B-C), with the option of selecting the most suitable color scheme to highlight specific features. For instance, in Figure 1B-C a temperature color scale is chosen to better distinguish electron denser (green) from less dense structures (red). The reconstructed 3D images gave a large sample overview with a voxel size of 130 nm and a more detailed view of selected regions of interest (voxel size of 50 nm).

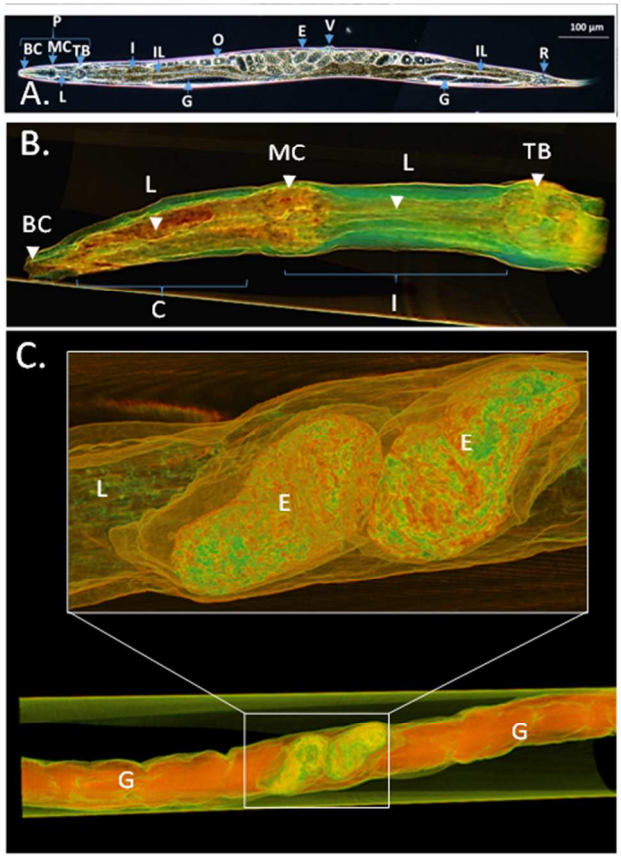

Figure 1. A.) Phase contrast microscopy showing C. elegans anatomy. The Pharynx (P) and upper digestive tract with Buccal cavity (BC), Meta corpus (Mc), Lumen (L),, Terminal bulb (Tb) (grinder). In the mid section of the nematode body, the intestine (I) with intestinal lumen(IL), gonads (G), oocytes (O) and fertilized embryos(E) inside the uterus, and vulva (V). At the anterior section, the intestinal lumen and the rectum (R) are annotated. . B.). Surface representation showing anatomical details of Pharynx and upper digestive tract based on 3D reconstructed phase contrast nano-CT with 50 nm voxel size. Buccal cavity (BC), Corpus (C), Meta corpus (MC), Lumen (L), Isthmus (I), Terminal bulb (TB) (also known as grinder). C.) Surface representation image of mid section of the nematode body showing the intestinal lumen (L), gonads (g) and fertilized embryos (E) inside the uterus. Image 1A used with permission of Erica Maremonti.

The same samples were subsequently scanned with XRF to obtain elemental distribution maps. Large overview maps were recorded with a step size of 400 x 400 nm^2, while a step size up to 10 x 10 nm^2 was used in order to visualize the finest details (e.g. Co-hotspots). A six element silicon drift diode

(SDD) detector was employed with a dwell time of 100 ms for each scanned pixel. 2D XRF tomograms (virtual cross-sections) were acquired with a lateral step size of 90 or 100 nm, angular steps of 0.3 degrees and a total rotation angle of 180 degrees. Semi-quantitative information on elemental concentrations was retrieved from the XRF signals for selected elemental distributions by calculating specific correction factors for various elements (such as Ca, Fe, Co and Zn). These factors correct for the differences in (i) attenuation by the capillary and (ii) the detector sensitivity for the various fluorescence energies as well as (iii) XRF sensitivity of each element for the primary X-ray beam. The attenuation caused by the sample (organic tissue) and the presence of (added) metals has not taken into account (see SI for more information).

Results and discussion

Cobalt Nanoparticles characterization.

In a previous study analytical TEM data from fresh batches of QSI-nano cobalt showed a size of 3.9 ± 0.8 nm (mean ± SD, n = 50) consisting of metallic cores in a close-packed, hexagonal structure with an amorphous Co_3O_4 shell with CoO in cubic structure in some places[17]. In the present study using synchrotron radiation (SR) based micro X-ray near edge structure (μ-XANES) spectroscopy and micro X-ray diffraction (μ-XRD) performed at beamline P06 (DESY) only Co_3O_4 was detected showing that the metallic Co had been oxidized (Supplemental Figure S5-S6).

The elemental composition of the NP was determined by ICP-MS (supplemental table S1). This showed that cobalt comprised 67% (w/w) of the total mass, which is what expected based on the XANES data, which showed presence of cobalt oxide (Co_3O_4). A number of elements were present in trace amounts (≤ 100 g/g), but the NP also contained significant amounts of boron (1.5% w/w) and calcium (0.34% w/w). The elemental purity and NP-aggregate size distribution was also analyzed by SR- XRF. The sum spectra revealed no major elements beside Cobalt in the NP (Fig S7-S8, table S2). The only significant contamination was Ni, which is consistent with the ICP-MS analysis (supplemental table S1).

The equilibrated Co-NP suspension was analyzed by dynamic light scattering (DLS) showing a zeta potential of -7.7 mV and size distribution of 185.8±70.1 nm d, accompanied by a small fraction of >1μm size aggregates (Figure S9). This is consistent with SR-analysis particle aggregate size estimated to 96 ± 42 nm^2 (n=10) (Figure S9).

Nano-CT at ID16A providing details of *C. elegans* at nm resolution

Whole individual nematodes were imaged in 3D with a voxel size of 130 nm and selected regions with a voxel size of 50 nm. This resulted in a typical measuring time of 4-8 hours per nematode. Such high-resolution images are required to allow linking the detection of foreign elements by XRF with their precise position in the nematode. For this kind of measurements, the sample preparation is crucial as the sample stability during the tomographic scans is essential for obtaining nanoscale 3D data. The procedure described in the methodology section met these requirements when the nematodes were mounted in quartz tubes. It should be noted that although PMMA tubes allow for the detection of low Z elements, the capillaries themselves are highly susceptible to beam damage.

Figure 1A provides an outline of the anatomy of *C. elegans*, familiarizing the reader with the terms that will be used hereafter. In Figure 1B-C we present holotomography results relative to specific nematode organs: pharynx with associated feeding organs in Fig. 1B; and intestine and uterus with fertilized embryos, located in the central part of the nematode, in Figure 1C.

Nano-XRF imaging of nematodes

As a first step 2D elemental distribution maps of entire individual nematodes or parts of them were acquired. Detailed elemental distributions of the pharynx and reproductive organs in non-exposed *C. elegans* are given in Figure 2 with Fe and Zn as main elements. The Zn distribution allows the visualization of morphological details, such as the oval shaped structures in Fig. 2B, which are embryos. Elements such as Zn and Fe are visible in the entire nematode body, but a dotted distribution of Zn and Fe hotspots was visible along the entire length of the intestine (Figure 2B). In *C. elegans,* Zn immobilization/storage vesicles are located intracellularly in the intestinal cells, and serve to maintain Zn homeostasis[28], by storing it when replete to avoid toxicity, and remobilizing it when needed[29]. The Fe granules are formed spontaneously in the intestinal cells in an age dependent manner, and their presence has been associated with senescence[30]. XRF elemental mapping performed with higher resolution (for instance in Fig. 3, 40 x 40 nm^2) revealed that the Zn granules did not feature a specific shape and had a typical diameter ranging between 50 to 150 nm. The Fe granules had a diameter of 100 nm at most.

Based on the natural Zn abundance in unexposed nematodes[31], an estimation of the Zn LOD was performed and resulted in about 0.01 fg/spot (20x37 nm^2) for 100 ms exposure. For cobalt the LOD estimation is expected to be similar due to the measurement conditions.

Several elemental distributions of the tail region of a Co-NP exposed and depurated nematode mounted in a PMMA capillary are shown in Figure 3. The use of PMMA capillaries allowed for detection of low atomic number elements such as phosphorous, sulfur, and calcium. The obtained data showed uneven and highly tissue specific distribution of essential elements such as Ca. Consistent with the distribution seen in Figure 3, calcium is involved in both enzymatic processes, in structural proteins, and as singling substance in most tissues and cells. For instance, neuronal activity (i.e. pharyngeal pumping foraging) is regulated via oscillating Ca^{2+} concentrations[18,28,19,30,31,32].

As anticipated in Figure 3, no clear association of any element with Co was visible in the exposed nematodes (further discussion in the following section). Background levels of Co were investigated and no Co was detected in the sum spectrum of the reference non-exposed nematode (Figure S10). Other trace elements were present in very low amounts, however local enrichments were seen for a few elements, such as copper in a ring-like structure in the transition between the buccal cavity and the procorpus (Fig 4B).

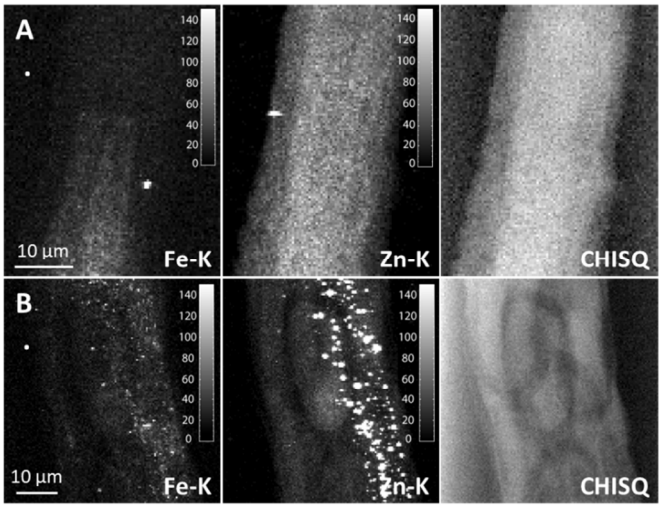

Figure 2. 2D XRF elemental distribution maps of the (A) pharynx lumen, 400 x 400 nm^2 step size, 36.8 x 57.2 µm^2 scan size and 100 ms exposure and (B) region surrounding the reproductive organs, 400 x 400 nm2 step size, 52.8 x 53.6 µm2 scan size and 100 ms exposure, of a non-exposed *C. elegans*. The Chi-square (CHISQ) distribution, which represents the difference between measured data and fitting function, is used to visualize the outline of the sample. Fitted intensity scales are shown as counts for each element.

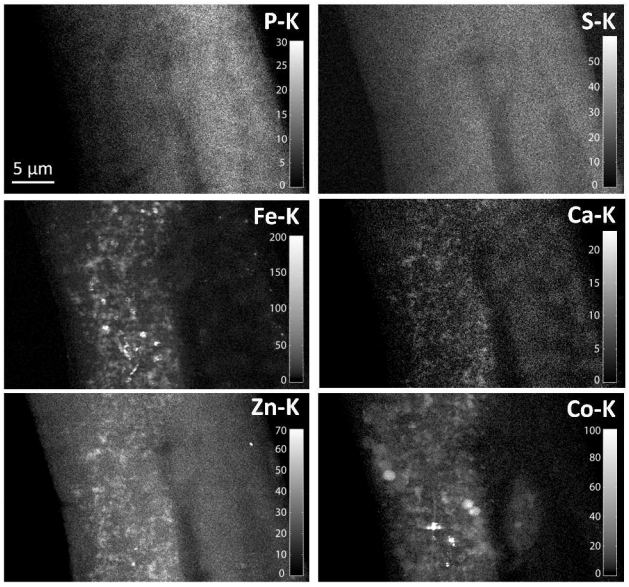

Figure 3. 2D XRF elemental distribution maps of the tail region of a Co-NP exposed and subsequently depurated *C. elegans* mounted in a PMMA capillary. XRF mapped area 36.2 x 22.3 µm^2, using 40 x 40 nm^2 step size and 50 ms dwell time per pixel. Fitted intensity scales are shown as counts for each element.

Co within the nematode: results from combined nano-CT and nano-XRF imaging

While the previous sections focused on the application of both techniques in terms of nematode imaging, the following one will deal more specifically with the investigation of Co present within the exposed nematodes.

The physiology of *C. elegans* is designed by evolution to localize and ingest micron-sized objects (bacteria). Chemosensory neurons enable their avoidance behavior or movement across chemical gradients, including certain inorganic ions. Their physiology can thus affect interaction and uptake of NP. The Co NP aggregates covered the surface (cuticle) of the nematodes during the exposure, but were efficiently removed from the body surface during depuration (results not shown).

Nematodes are known to be able to separate bacteria from other particles in the pharynx[33]. However, we observed that NP aggregates were ingested together with the bacteria (arrows in Figure 4A). The Zn distribution in Fig. 4B can be used as an outline of the outer boundaries of the nematodes, and anatomical features can be identified by comparison with Fig. 1A. For instance, it can be seen how Zn is more concentrated in the lower part of the figure, i.e. the anterior part of the intestinal lumen. When looking at the Co-distribution in the pharynx in Fig. 4B, Co-particles are mostly abundant in the center of the lumen between metacorpus and terminal bulb (grinder) and in the grinder itself (Figure 4B - blue box, Figure 4C). In the isthmus, only a few NPs were present, while aggregates were abundant in the grinder and in the anterior part of the intestine, i.e. close to the. Such a pattern is consistent with normal *C. elegans* filter feeding behavior[34]. To investigate the location of particles in the different tissues, XRF tomography was performed on a section in the anterior intestine (Figure 4D). The tomographic reconstruction showed elemental distributions in a virtual cross-section of the nematode. The Zn distribution shows the outline of the nematode body. The slightly lighter blue color at the center corresponds to the intestinal lumen. The Co (red) and Fe (green) were present as small hotspots located in the intestine and the intestinal lining. The linear elongation of the hotspots is an artefact due to slight sample movement caused by heating of the sample.

The Co-NP distribution in the mid gut section of the nematode was investigated by 2D-XRF mapping on two nematodes that had been subjected to depuration subsequent to exposure as well as on non-depurated nematodes. Individual aggregates of NPs were visible throughout the length of the intestinal lumen of the non-depurated nematode (Figure 5). NPs were also readily detected in the intestine of the exposed and depurated nematodes (Figure 4B-C).

During normal feeding behavior the nematode defecation cycle is 50 seconds[35]. Therefore, digestion and assimilation of nutrients occur throughout the entire intestine within a short period. While Co-NP aggregates were less abundant than in the non-depurated nematode, the presence of Co-aggregates in the intestine after depuration thus indicates a strong binding or uptake of particles by the intestinal cells (Figure S13). The high abundance of Co observed in the nematode prompted us to investigate whether the NPs were confined to the intestinal lumen or if they were translocated into other parts of *C. elegans*. Detailed maps (40-100 nm resolution) showed aggregates with diameters up to 200 nm in both non-depurated (Figure 5B-C) and depurated animals (Figure 4B-C).

In fact, a large portion of Co was aligned with the intestinal epithelium and distinct Co-globules of Co-aggregates appeared to be embedded in the intestinal cells tissue in a similar fashion as the Zn and Fe spotty distribution (Figure 5B). However, the images showed distinct patterns in close proximity to Zn and Fe granules in the intestinal cell vesicles, and Co hotspots did not co-localize with either element (Figure 5B). This is confirmed by a Zn-Co correlation plot

(Figure S11). This suggests that Co-NP were not stored in the gut granules described in the previous section[20]. Furthermore, Co-NPs occupied a wider section of the nematode body than the Zn or Fe granules, confirming the presence of Co-NPs outside the intestine cavity.

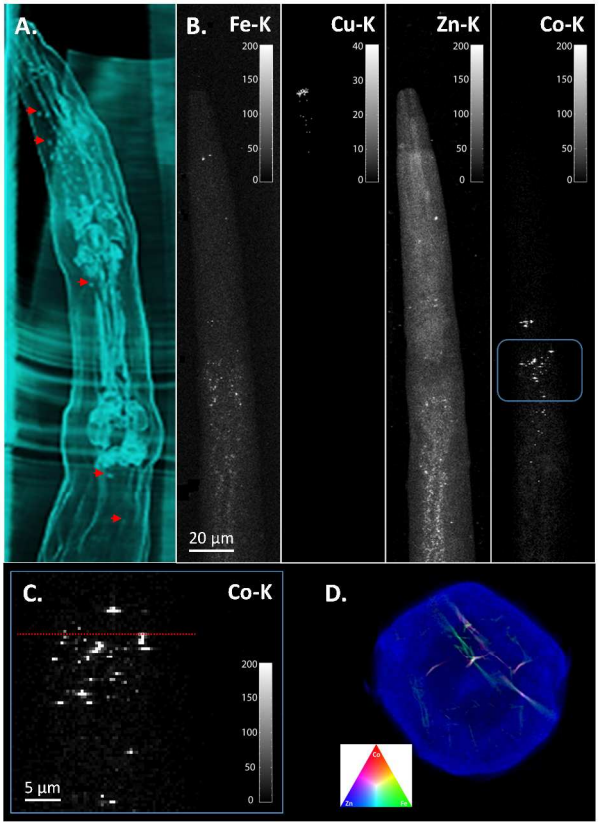

Figure 4. A.) Three dimensional (3D) reconstructed phase nano-CT image of the nematode pharynx of an exposed non-depurated specimen. Arrows indicate the position of suspected NP aggregates. B.) 2D XRF elemental distribution maps of a depurated animal. Step size 400 x 400 nm^2, scan size 46.4 x 247.6 µm^2, 100 ms dwell time per pixel. The blue box in the area between lumen and terminal bulb (see Fig 1A) indicates the high resolution mapped area. C.) Close view of section posterior to pharyngeal/intestinal valve. (D.) 2D XRF tomogram (position of the virtual cross-section indicated by the red line in C) of Zn (blue), Fe (green) and Co (red), demonstrating the presence of Co-NPs in the anterior part of the intestine.

An important aspect of NP-toxicity is whether or not the effect of NP-exposure could affect reproduction. Several studies have reported reproductive defects and transfer of NPs to embryos[21,22,23]. Thus, the presence of Co-NPs outside the intestinal lumen as demonstrated by 2D –(tomo)XRF needed additional investigation on whether Co-NPs could be translocated from the lumen into the developing embryos of the nematode.

Therefore, we focused on the area surrounding the uterus and the embryos and we selected Co-aggregates localized in close proximity to the gonads or embryos for further investigation. By rotating the specimen 90° and scanning the sample from this angle, we identified single candidate areas where particles had a position consistent with the embryos (Figure 5C).

A region of interest (ROI) is shown in a CT rendering in supplemental Figure S12. Two areas, which intercept the surface of the embryos, were selected for high resolution 2D XRF mapping (Figure S12B-C). Both of these areas revealed Co-NPs that have potentially translocated into the uterus, as can be seen from the Co distribution in Figure S12B and 12C.

The two candidate Co-NP aggregates were selected as a case study. To investigate the position of the aggregates inside the nematode, an approach involving a combination of phase contrast nano-CT and XRF was devised. First, a longitudinal virtual slice was obtained by phase contrast nano CT in (Figure 6A). A high resolution 2D XRF projection map of Co corresponding to the ROI was constructed (Figure 6B) to verify the identification of the suspected Co-NPs. Since these are 2D projections, a nano-CT projection in the XY-plane was constructed to confirm the position of these aggregates within the embryo (Figure 6C). Finally, the temperature color scale in Figure 6D allows to enhance the contrast between the aggregate and the surrounding tissues. Notably, the size of the two aggregates were large (approximately 1.4 µm diameter in XRF maps and 1.8 µm in the tomograms). All the above strongly supports the identification of the two structures in the virtual slice as the two Co aggregates. However, one cannot completely exclude that, as already commented for Figure 4D, co-localization of these signals is an artefact due to slight sample movement caused by heating of the sample.

Further, Co-NP were investigated by employing phase contrast renderings, enabling 2D and 3D visualization of the NP-aggregates (Figure S13). Individual NP-aggregates varying between 50-200 nm (diameter) were visible in the intestine. Although the majority of Co-NPs were found within the intestine, a fraction of NP-aggregates appeared as translocated to the uterus and embryos and in proximity to the embryos Figure S13B shows a virtual longitudinal section of both the intestine and the embryos inside the uterus. This section showed oval shaped protruding structures on the embryo surface, of which electron density and size are consistent with the NP-aggregates shown in Figure 6.

Conclusion

This study has generated the highest resolution 2D and 3D images so far in NP uptake studies (50 nm voxel size for CT, 40 nm pixel size for XRF). Only such highly detailed morphological and elemental images allow for the identification of NPs in reproduction relevant areas of the organisms. Although the resolution is insufficient for identifying single nanoparticles, we have demonstrated that Co NPs are predominantly present as aggregates in the nematode tissues and, we have demonstrated efficient uptake of Co-NPs in different parts of the nematodes, NP tightly bound to the intestinal epithelium and presumably translocation to the reproductive organs.

The nano-analytical capabilities of ESRF beamline ID16A have proven to be useful to image clusters of Co nanoparticles in nematodes using phase contrast CT and nano-XRF imaging. Several limitations of this experiment can be overcome following the acquired experience in terms of sample preparation and after the recent developments on the beamline. These include improved spatial resolution[7] thanks to better sample stability during the scan, improved image quality both in fluorescence CT and phase contrast CT thanks to optimized acquisition strategies and better sample preservation via a newly installed cryogenic system.

In this study we have established a system for nm resolution non-invasive image analysis of the internal distribution of essential and toxic elements in an intact animal using *C.*

elegans as a model. Therefore, this study paves the way for further nanotoxicology investigations based on the same techniques.

AUTHOR INFORMATION

Corresponding Author

* simone.cagno@nmbu.no
$ SC and DAB contributed equally to this work.

Author Contributions

The manuscript was written through contributions of all authors. All authors have given approval to the final version of the manuscript.

Supporting Information (SI) available, with information on: ID16A beamline; Synchrotron radiation based micro X-ray speciation techniques; Attenuation correction; Preparation of Cobalt NanoParticle (NP) suspensions; Inductively coupled plasma mass spectrometry (ICP-MS); Dynamic light scattering DLS and Zeta potential; Cobalt Nanoparticles (Co NPs) characterization; Cobalt-NP suspension characterization; Background level of Co in the unexposed nematode; Exposed nematodes; Additional results not shown in the main paper.

ACKNOWLEDGMENT

This study has been funded by the Norwegian Research Council through its Centre of Excellence (CoE) funding scheme (Project No. 223268/F50). We gratefully acknowledge ESRF and DESY for granting beamtime and Karl Andreas Jensen for performing ICP-MS analysis. We thank Erica Maremonti for supplying phase contrast image used in Fig 1A.

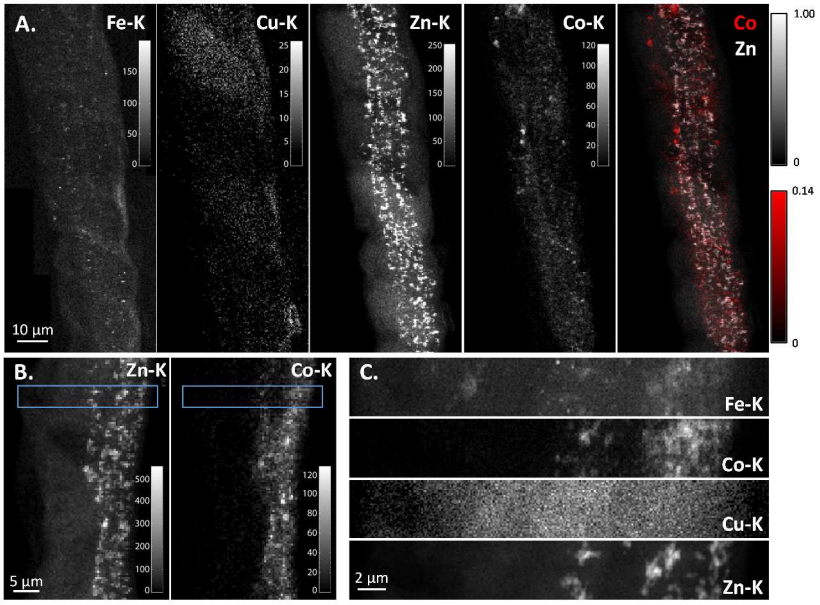

Figure 5. Two dimensional X-ray mapping of an exposed non-depurated nematode intestine and surrounding tissues. (A.) Coarse 2D-XRF element distribution maps of Fe, Cu Zn, and Co using 400 x 400 nm^2 step size, 49 x 113 µm^2 scan size and 100 ms exposure. Right panel, showing Co spatial distribution and intensity relative to Zn. (B.) Sample rotated 90^0 degrees, Coarse 2D-XRF element distribution maps 400 x 400 nm2 step size, 35 x 47 µm^2 scan size, and 100 ms exposure indicating Co in proximity to embryos. (C) Fine 2D-XRF elemental distribution maps (100 x 100 nm^2 step size, 28 x 4 µm^2 scan size, 200 ms dwell time per pixel) of transversal section showing majority of Co associated with intestinal tissues but also located in proximity to embryo. Intensity scales are shown as counts for each element.

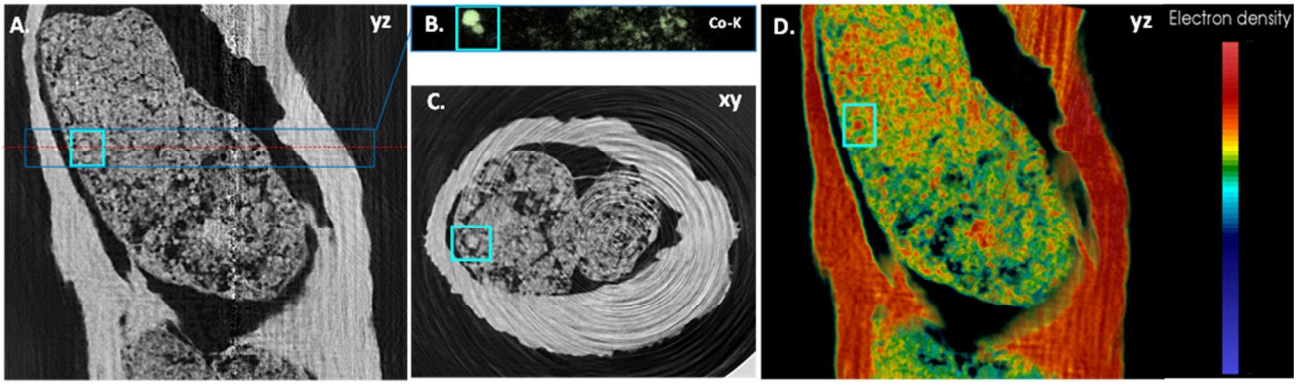

Figure 6. Identification and localization of NP (magenta box) inside embryo by combined phase contrast nano-CT and XRF. (A). Phase contrast nano-CT (voxel size 50 nm) longitudinal virtual slice (yz) showing Co-NP aggregate. (B). 2D-XRF Co element distribution map of the section indicated by blue box (ROI: 32.6 x 4.0 μm^2; step size: 40 nm). (C). Phase contrast nano-CT transversal virtual slice (xy), dotted red line indicates in the longitudinal virtual slice marks it's the position. (D) Virtual slice with temperature color scale of the uterus and embryos.

TOC graphic

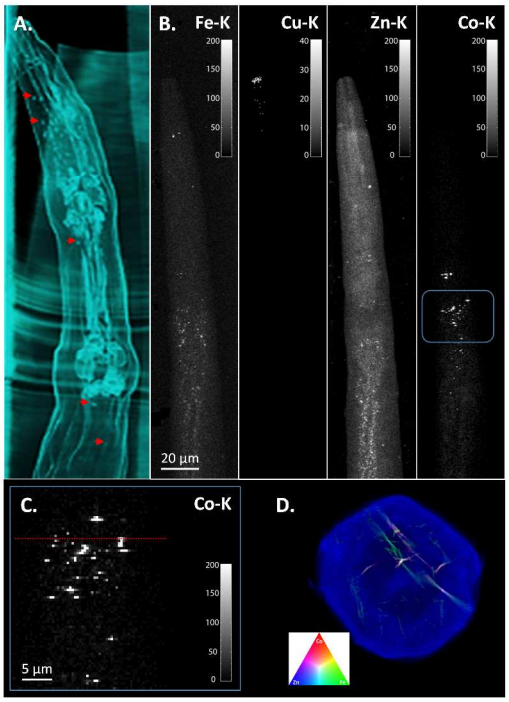

REFERENCES

1. Zhu, Y.; Cai, X.; Li, J.; Zhong, Z.; Huang, Q.; Fan, C.; Nanomedicine 2013, 10, 515-524.
2. De Samber, B.; Silversmit, G.; Evens, R.; De Schamphelaere, K.; Janssen, C.; Masschaele B.; Van Hoorebeke, L.; Vanhaecke, F.; Falkenberg, G.; Vincze, L. et al.; Desy Annual Report 2007, 2008, 1291-1292.
3. Chen, C.; Li, Y.F.; Qu, Y.; Chai, Z.; Zhao, Y.; Chem Soc Rev. 2013, 42, 8266-8303.
4. Li, Y.; Li, Y.F.; Zhao, J.; Gao, Y.; Chen, C.; J. An. At. Spectrom. 2015, 30, 2038-2047.
5. Deng, J.; Vine D.J.; Chen, S.; Nashed, Y.S.G.; Jin, Q.; Phillips, N.W.; Peterka, T.; Ross, R.; Vogt, S.; Jacobsen, C.J.; Proc Natl Acad Sci U S A. 2015, 112, 2314-2319.
6. Martinez-Criado, G.; Vilanova, J. ; Tucoulou, R. ; Salomon, D. ; Suuronen, J.P. ; Laboure, S. ; Guilloud, C.; Valls, V.; Barrett, R.; Gagliardini, E.; et al.; J. Synchr. Rad. 2016, 23, 344-352.
7. Da Silva J.C.; Pacureanu, A.; Yang, Y.; Bohic, S.; Morawe, C.; Barrett, R.; Cloetens, P.; Optica 2017, 4, 492-495.
8. Schroer, C.; Boye, P.; Feldkamp, J.; Patommel, J.; Samberg, D.; Schropp., A.; Schwab, A.; Stephan, S.; Falkenberg, G.; Wellenreuther, G. et al.; Nucl Instrum Methods Phys Res A 2010, 616, 93-97.
9. De Samber, B.; De Schamphelaere K.A.; Janssen C.A.; Vekemans, B.; De Rycke, R.; Martinez-Criado, G.; Tucoulou, R.; Cloetens, P.; Vincze, L.; Anal. bioanal. Chem. 2013, 405, 6061-6068.
10. Nowack, B.; Bucheli, T.D.; Environmental pollution 2007, 150, 5-22.
11. Robinson, I.; Yang, Y.; Zhang, F.; Lynch, C.; Yusuf, M.; Cloetens, P.; J. SynchrotronRadiat. 2016, 23, 1490-1497.
12. Oughton, D.H.; Hertel-Aas, T.; Pellicer, E.; Mendoza, E.; Joner, E.J.; Environ. Toxicol. Chem. 2008, 27, 1883-1887.
13. Coutris, C.; Hertel-Aas, T.; Lapied, E.; Joner, E.J.; Oughton, D.H.; Nanotoxicology 2012, 6, 186-195.
14. Colvin, V.L.; Nat. Biotechnol. 2003, 21, 1166-1170.
15. Legrand, J.; Petit, C.; Pileni, M.; J. Phys. Chem. B 2001, 105, 5643-5646.
16. Gonzales-Moragas, L.; Roig, A.; Laromaine, A.; Adv Colloid Interface Sci. 2015, 219, 10-26.
17. Maddox, A.S.; Maddox P.S.; Methods Cell Biol. 2012, 107, 1-34.

18. McColl, G.; James, S.A.; Mayo, S.; Howard, D.L.; Ryan, C.G.; Kirkham, R.; Moorhead, G.F.; Paterson, G.; De Jonge, M.D.; Bush , A.I.; PLoS One 2012, 7, e32685.
19. James, S.A.; De Jonge, M.D.; Howard, D.L.; Bush, A.I.; Paterson, D.; McColl, G.; Metallomics 2013, 5, 627-635.
20. Hare, D.J.; Jones, M.W.; Wimmer, V.C.; Jenkins, N.L.; De Jonge, M.D.; Bush, A.I.; McColl, G.; Metallomics 2016, 8, 156-160.
21. Pluskota, A.; Horzowski, E.; Bossinger, O.; Von Mikecz, A.; PLoS ONE 2009, 4, e6622.
22. Meyer, J.N.; Lord, C.A.; Yang, X.Y.; Turner, E.A.; Badireddy, A.R.; Marinakos, S.M.; Chilkoti, A.; Wiesner, M.R.; Auffan, M.; Aquat. Toxicol. 2010, 100, 140-150.
23. Qu, Y.; Li, W.; Zhou, Y.; Liu, X.; Zhang, L.; Wang, L.; Li, Y.F.; Iida, A.; Tang, Z.; Zhao, Y. et al.; Nano Lett. 2011, 11, 3174-3183.
24. Starnes, D.L.; Unrine, J.M.; Starnes, C.P.; Collin, B.E.; Oostveen, E.K.; Ma, R.; Lowry, G.V.; Bertsch, P.M.; Tsyusko, O.V.; Environmental Pollution 2015, 196, 239-246.
25. Tyne, W.; Lofts, S.; Spurgeon, D.J.; Jurkschat K.; Svendsen, C.; Environ Toxicol Chem. 2013, 32, 1711-1717.
26. International Organization for Standardization, 2010, *ISO 10872:2010 Water quality -- Determination of the toxic effect of sediment and soil samples on growth, fertility and reproduction of Caenorhabditis elegans Nematoda*.
27. Mokso, R.; Cloetens, P.; Applied physics letters 2007. 90, 144104.
28. Espelt, M.V.; Estevez A.Y.; Yin, X.; Strange, K.; J. Gen. Physiol. 2005, 126, 379-392.
29. Roh, H.C.; Collier, S.; Guthrie, J.; Robertson J.D.; Kornfeld, K.; Cell Metab. 2012, 15, 88-99.
30. James, S.A.; Roberts, B.R.; Hare, D.J.; De Jonge, M.; Birchall, I.E.; Jenkins, N.L.; Cherny, R.A.; Bush, A.I.; McColl, G.; Chem. Sci. 2015. 6, 2952-2962.
31. Ganio, K.; James, S.A.; Hare, D.J.; Roberts, B.R.; McColl G.; Analyst 2016, 141, 1434-1439.
32. Teramoto, T.; Iwasaki, K.; Cell Calcium 2006, 40, 319-327.
33. Fang-Yen, A.C.L; Samuel A.D.; Proc Natl Acad Sci USA 2009, 106, 20093-20096.
34. Avery, L.; Shtonda, B.B.; J Exp Biol. 2003, 206, 2441-2457.
35. Dal Santo, P.; Logan, M.A.; Chisholm, A.D.; Jorgensen, E.M.; Cell 1999, 98, 757-767.